Arch Appl Mech (2019) 89:919–926
https://doi.org/10.1007/s00419-018-1435-1

ORIGINAL

E. Džindo · S. A. Sedmak · A. Grbović · N. Milovanović · B. Đorđević

XFEM simulation of fatigue crack growth in a welded joint of a pressure vessel with a reinforcement ring

Received: 6 March 2018 / Accepted: 19 July 2018 / Published online: 7 December 2018

Abstract The numerical analysis of the behaviour of a pressure vessel with a reinforcement ring subjected to both static and dynamic load is presented in this paper. This research was based on a previous analysis which involved different reinforcement ring dimensions, and their influence on the stress distribution within the pressure vessel, assuming the presence of a crack (Sedmak et al., in: International Conference on Structural Integrity and Durability, 2017). The aim was to compare the numerical results for two models, one of which was a 2D model simulated with classic FEM, whereas the other included a 3D fatigue crack, and was simulated with extended finite element method, using Morfeo software. The numerical simulation was based on a pressure vessel which is typically used as a part of hydropower plants, containing a manhole which is supported by the reinforcement ring. The analysis focused on a crack that was located in the welded joint between the reinforcement ring and the pressure vessel mantle. The results obtained by the simulations have shown the differences in the stress magnitudes and in the consequences resulting from the crack growth in both cases, depending on the type of the load, wherein the second (fatigue) load case was noticeably more extreme.

Keywords Pressure vessel · Stress intensity factor · XFEM · Fatigue · Reinforcement ring

1 Introduction

Typically, pressure vessels contain various connections to pipelines, as well as manholes, whose purpose is to enable maintenance and repairs when necessary. Such openings need to be adequately reinforced along their circumference, to account for the stress concentration resulting from the changes in the vessels geometry at these locations [2]. These connections are often made by welding different types of materials, and due to this the behaviour of such welded joints is of particular interest, because of their heterogeneous nature, which, along with the changes in the geometry, lead to significant stress concentrations [3–5].

In this study, the crack was introduced to a welded joint connecting the reinforcement ring to the wall of the pressure vessel in order to determine its behaviour under the load corresponding to the working and test pressures. In addition, another model was made, which simulated the crack growth under fatigue load, for the purpose of comparing the stress/strain distribution to determine how different load conditions affect the integrity of the pressure vessel, in terms of crack behaviour, since fatigue has considerable effect of the integrity of pressure equipment, and it should be taken into account for this reason [6]. For this purpose, both classic and extended finite element methods (XFEM) were used.

E. Džindo · S. A. Sedmak (✉) · N. Milovanović · B. Đorđević
Innovation Center of Faculty of Mechanical Engineering, Kraljice Marije 16, Belgrade 11120, Serbia
E-mail: simon.sedmak@yahoo.com
Tel: +381 62 295 496

A. Grbović
Faculty of Mechanical Engineering, Kraljice Marije 16, Belgrade 11120, Serbia

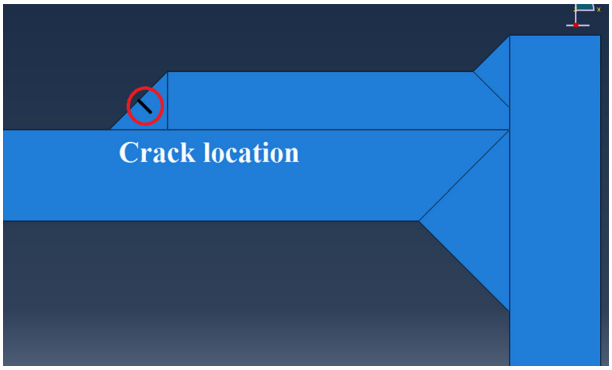

Fig. 1 Location of the 5-mm crack in the first numerical model (between the reinforcement ring and the pressure vessel mantle)

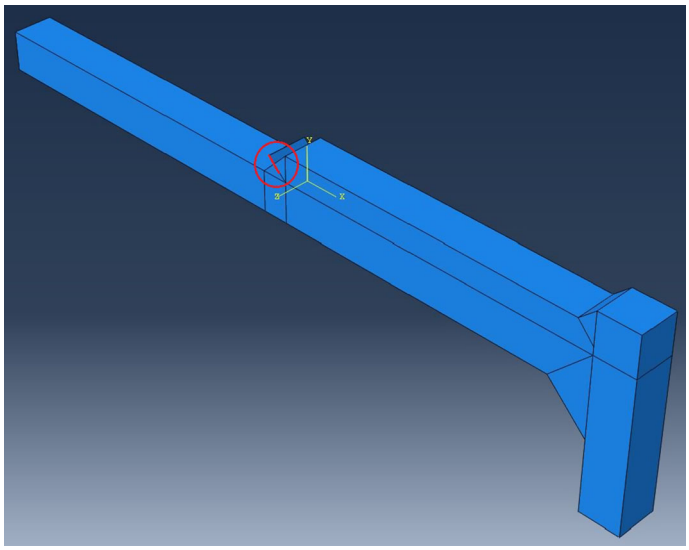

Fig. 2 Location of the 5-mm crack in the second numerical model (between the reinforcement ring and the pressure vessel mantle)

Table 1 Mechanical properties of the pressure vessel and manhole materials used in the simulation

Material	Yield strength, R_e (MPa)	Tensile strength, R_m (MPa)	Elasticity module (MPa)	Poisson's ratio
S275JO	313	472	200,000	0.3
P 280 GH	300	350	210,000	0.3
EVB50	440	510	210,000	0.3

2 Finite element models

Pressure vessel walls were made from S275JO steel, whereas the reinforcement ring was made using steel P 280 GH. Electrode EVB50 was used as filler material for welded joints. The crack location was the central section of the weld between the S275JO and P 280 GH steel (the pressure vessel mantle and the reinforcement ring respectively), as can be seen in Fig. 1. Initial crack length was 5 mm. Figure 2 shows the crack location and the geometry of the 3D model, used for the fatigue simulation.

Shown in Table 1 are the mechanical properties of the three materials that were used for the pressure vessel and the welded joint.

Shown in Fig. 3 is the actual pressure vessel with the manhole on which the model was based, whereas Fig. 4 shows a part of the documentation where some of the dimensions can be seen.

Fig. 3 The pressure vessel with the manhole cover

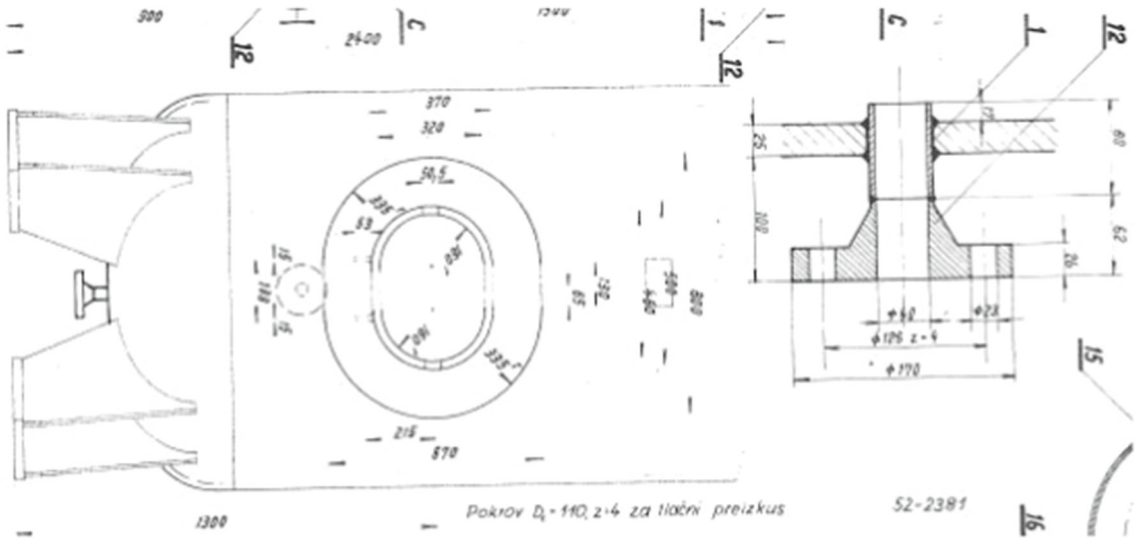

Fig. 4 Sketches of the pressure vessel and the manhole cover, taken from the documentation

The numerical simulation of the first model was performed using finite element method [7], whereas the second model was analysed using XFEM. The extended finite element method is a recently developed method used for numerical simulation of crack growth. It involves the use of so-called enrichment functions, whose purpose is to improve the typically used interpolation functions, while maintaining the concept of partition of unity [8]. The greatest advantage of XFEM compared to the classic finite element method is that there is no need to remesh the model during the simulation. Instead, the enrichment functions allow the finite elements to be used in a way that eliminates the discontinuities in the model, which are typically the consequence of cracks. Enriched functions are given in the following from:

$$u^h(x) = \sum_i N_i(x) \Big| u_i + \sum_j v^j(x)\, a_i^j \tag{1}$$

where $u^h(x)$ represents the classic degrees of freedom of a finite element, the first sum in the equation represents the classic interpolation function, and the second sum is the enrichment function [6]. XFEM application requires the use of special types of elements and nodes, which can be distinguished by the type way in which the finite element nodes are generated. Two most frequently used types are the near-tip nodes and Heaviside nodes. An example of a crack represented by such finite elements is shown in Fig. 5.

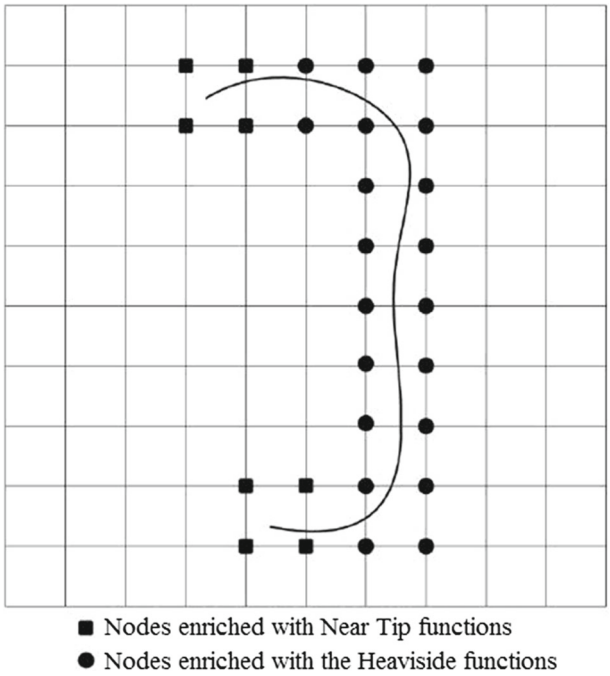

Fig. 5 Extended finite element mesh using different types of enrichment functions

Table 2 Finite elements used in static and dynamic load models

Model	Element type	Number of elements	Number of nodes
First (static load)	CPS4R	15,403	25,981
Second (fatigue)	C3D8R	27,050	51,678

ABAQUS software (Dassaúlt, France) was used for both models. In addition, Morfeo software, an extension for ABAQUS used in fatigue simulations, was employed for the second analysis. For this reason, the second model had to be made as 3D, unlike the first one which could be simulated in two dimensions.

For the first model, the load was defined as a 50 bar (5 MPa) internal pressure, in accordance with the test pressure defined in the documentation. For the second model, the load was defined with the same magnitude, but was applied as dynamic, to simulate the fatigue behaviour of the model. Since Morfeo performs its calculations based on the Paris equation, ($\frac{da}{dN} = C(\Delta K)^m$) [9], the following values of coefficients C and m were adopted, for the materials used: $C = 3.5$, $m = 10^{-12}$.

The type of finite elements adopted for both models, along with their number and the number of nodes, is shown in Table 2:

The materials used for the first model were defined both in terms of elastic and plastic behaviour, based on their mechanical properties. In the case of the second model, plastic behaviour was excluded, since fatigue crack growth in this case was observed from the standpoint of linear-elastic fracture mechanics.

The boundary conditions and the loads are shown in Fig. 6. The boundary condition on the left side corresponds to the location where the model segment was "cut" from the pressure vessels; thus, translation along both axes was prevented. The boundary condition on the right upper end was added to simulate the presence of the manhole cover, which would prevent movement along the x-axis. In the second model, the load was defined in the same way, along the bottom surfaces, whereas the boundary conditions are shown in Fig. 7. Both constrained surfaces were only allowed rotation along the Z-axis, which corresponds to the way in which the actual pressure vessel would deform and which would result in the possibility of crack growth.

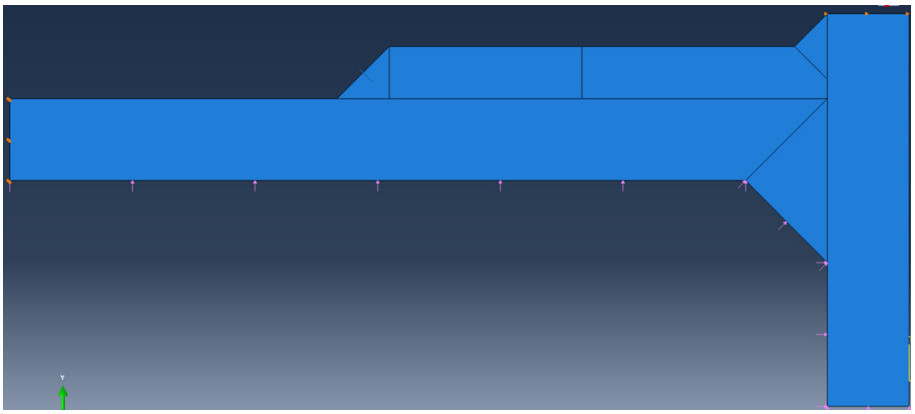

Fig. 6 The load and boundary conditions of the 2D model

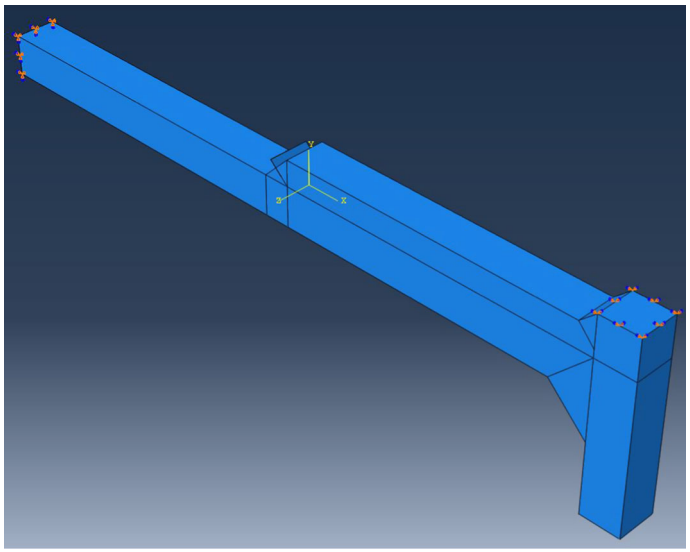

Fig. 7 Boundary conditions of the 3D model

3 Results

The results of the numerical simulations are shown in Figs. 8 and 9, showing the stress distribution and crack growth in the 2D and 3D models, respectively. As was expected, the stresses in the second model were noticeably higher, and the crack propagated significantly compared to the static model, wherein the plastic strain was very small.

In addition, the results for the fatigue behaviour, in terms of the stress intensity factor and the number of cycles for the second model, in accordance with the previously defined Paris equation parameters, are shown in this section, Table 1 and Fig. 10.

Figure 4 shows a more detailed view of the welded joints itself, wherein the behaviour of the crack can also be observed. The left image is that of the first model, whereas the right one corresponds to the second. It can be seen that the applied load (working pressure) did not significantly affect the initial length of the crack.

4 Discussion

This paper involved the numerical analysis of the crack growth behaviour in two models, one of which was a 2D model subjected to static load and the other which was a 3D model subjected to fatigue. Both models

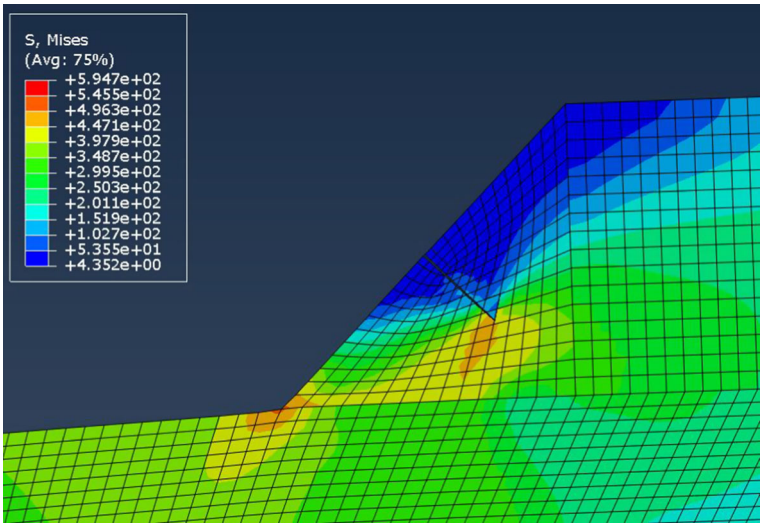

Fig. 8 Stress distribution for the first model in the welded joint area

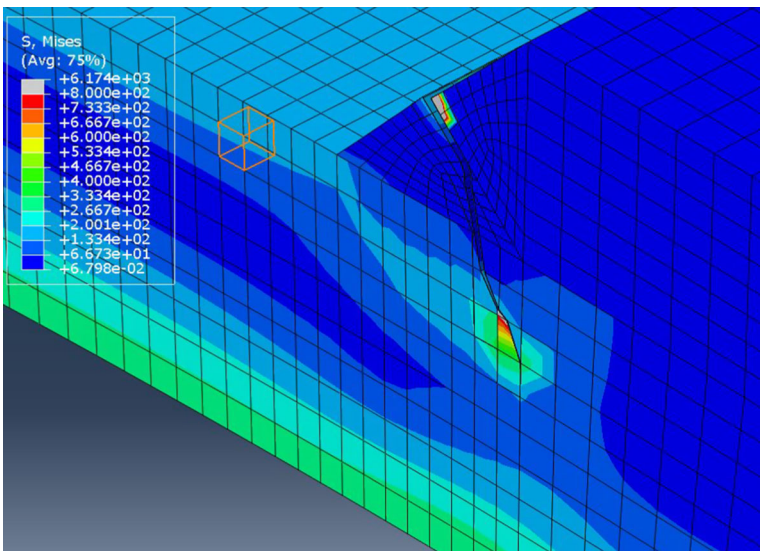

Fig. 9 Stress distribution and crack propagation in the second (XFEM) model

included a crack with the initial length of 5 mm, located in the centre of the welded joint between the mantle and the reinforcement ring. In the case of the first model, the highest stresses were located at the connection of the bottom edge of the welded joint and the mantle, as well as around the crack tip, with magnitudes of 545.5 and 496.3 MPa, respectively (disregarding the stress values near the supports). The crack itself did not grow significantly, and the plastic strain in the model was minimal.

For the second model, the stresses have reached noticeably higher levels, as expected, since the load was applied as dynamic. Stresses near the crack tip had exceeded 800 MPa, and the model ultimately failed after 56,290 load cycles. Due to the extreme load, the crack propagated through the welded joint and into the parent metal (P 280 GH), which was a result of the crack length and the weld metal geometry, as well as the fact that the WM (EVB50) is stronger than the parent material (yield strength of 440 MPa compared to 300 MPa, which is the yield strength of P 280 GH). The length of the crack in the final step was 17.678 mm. Shown in Table 3 and Fig. 10 are the values of the stress intensity factor for each step, along with the number of cycles corresponding to them.

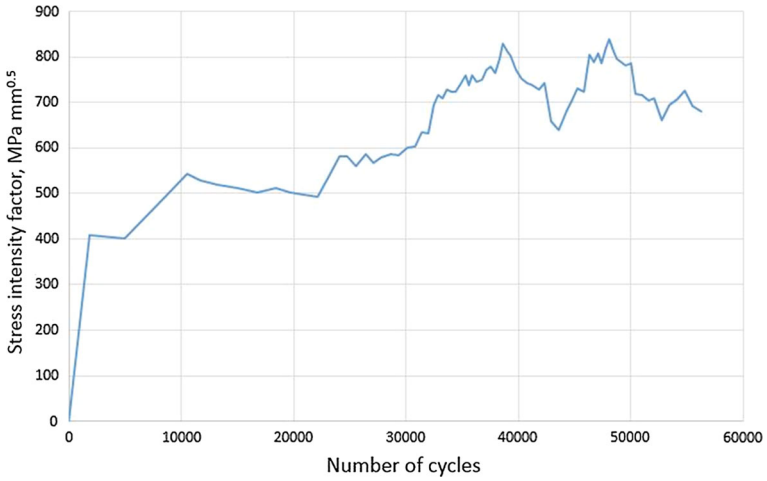

Fig. 10 Stress intensity factor versus number of cycles

Table 3 Cycles and SIFs for each XFEM simulation step

Step	Cycles	SIF	Step	Cycles	SIF
1	0	0	40	37530.66	779.949
2	1843.99	408.556	41	37912.82	764.515
3	4924.86	402.121	42	38300.16	796.406
4	8374.91	486.767	43	38644.95	829.881
5	10473.54	542.546	44	38972.05	812.956
6	11681.82	528.838	45	39334.57	801.756
7	13243.37	517.799	46	39758.72	772.492
8	14955.37	512.012	47	40242.14	752.527
9	16751.74	503.045	48	40754.92	743.314
10	18357.86	512.254	49	41288.55	736.793
11	19649.02	502.925	50	41843.04	729.324
12	20855.61	497.033	51	42359.28	741.932
13	22128.83	493.092	52	42909.81	658.235
14	23219.53	540.344	53	43587.66	640.073
15	24021.46	580.912	54	44230.32	679.66
16	24751.83	581.444	55	44781.73	703.991
17	25564.97	559.496	56	45293.67	730.412
18	26374.82	586.36	57	45798.05	722.511
19	27079.03	567.459	58	46276.48	804.56
20	27821.35	579.589	59	46692.03	789.416
21	28611.17	586.345	60	47065.52	807.667
22	29380.81	583.881	61	47429.44	785.82
23	30094.69	599.641	62	47789.73	819.05
24	30785.92	602.312	63	48123.29	839.905
25	31421.11	633.666	64	48459.46	811.887
26	31983.4	631.11	65	48807.08	794.916
27	32474.42	694.0921	66	49183.56	789.678
28	32860.61	715.921	67	49585.86	781.256
29	33240.67	708.876	68	49998.55	786.477
30	33622.91	729.198	69	50461.54	718.537
31	34010.32	724.434	70	50986.34	715.809
32	34426.42	723.559	71	51559.98	703.53
33	34862.79	742.759	72	52103.42	708.203
34	35252.54	759.29	73	52723.22	660.441
35	35595.81	738.457	74	53447.64	694.029
36	35900.91	758.829	75	54139.27	707.497
37	36274.93	745.426	76	54788.5	726.112
38	36718.85	750.89	77	55473.28	693.408
39	37134.2	771.455	78	56290.4	679.644

The results from the above figure show a significant deviation from the expected shape of the curve, as a consequence of the crack propagation into the parent material, where the mesh was not refined to the expected extent. However, this was not needed, since the stress intensity factors were already above the fracture toughness of used materials, due to the extremely conservative approach. Nonetheless, the results suggest that considerable improvements should be made to the existing model. The noticeable jump in the SIF values after 30,000 cycles corresponds to the moment wherein the crack propagated into the parent material, whose mechanical properties are below those of the weld metal, as previously mentioned. The fatigue load in this study was adopted in the following way (the static and dynamic pressure magnitudes were the same, although it is typical to adopt lower values of load for dynamic cases) in order to ensure that the fatigue crack would propagate, for the purpose of comparing it with the static case.

5 Conclusion

The results shown here are meant to be used as a basis for further research, and there is still a lot of room for improvement of the model. In addition, the Paris law parameters were adopted based on the literature, instead of being determined experimentally, as recommended.

The results obtained in this paper indicate that it is possible to quickly and efficiently compare models subjected to different load cases, although it should be mentioned that these models were also heavily approximated; thus, further work should focus on creating more realistic, optimised models. It also showed the potential issues that can be encountered, and the ways in which they can be improved, in order to obtain more accurate results. In addition to adequate defining of boundary conditions, the size of finite elements in the areas where the crack is expected to propagate should be taken into account, and such simulations should be based on experimental results, especially in terms of Paris law parameters.

Further research of this subject should involve the actual experimental determination of Paris coefficients C and m for the weld metal. Additionally, failure assessment diagrams should be made, after a more realistic fatigue load is adopted for future models, as drawing them in this extremely conservative model would not provide any significant insight into the behaviour of the pressure vessel.

Acknowledgements The authors of this paper would like to express their gratitude to the Ministry of Education, Science and Technological Development of Republic of Serbia for the support of projects TR35040 and TR35011.

References

1. Sedmak, S.A., Milovanović, N., Džindo, E., Đorđević, B., Tatić, U.: Numerical simulation of the influence of reinforcement ring on stress and strain distribution in pressure vessels. In: International Conference on Structural Integrity and Durability, pp. 167–168 (2017)
2. EN 13445-3:2014 (E) Issue 1 (2014-09)
3. Skopinsky, V.N., Berkov, N.A., Vozhov, R.A.: Effect of pad reinforcement on the plastic limit load for nozzle connection of cylindrical vessel. J. Press. Vessel Technol. **137**(2), 021207 (2014)
4. Radu, D., Sedmak, A.: Welding joints failure assessment—fracture mechanics approach. Bull. Transylv. Univ. Brasov Ser. I Eng. Sci. **9**, 119–126 (2016)
5. Arsić, M., Bošnjak, S., Sedmak, S.A., Šarkočević, Ž., Savić, Z., Radu, D.: Determination of damage and repair methodology for the runner manhole of Kaplan turbine at the hydro-power plant "Djerap 1". Struct. Integr. Life **16**(3), 149–153 (2016)
6. Hobbacher, A.: Recommendations for Fatigue Design of Welded Joints and Components. Springer (2016)
7. Maneski, T.: Kompjutersko modeliranje i proračun struktura, Mašinski Fakultet Univerziteta u Beogradu (1998)
8. Khoei, A.R.: Extended Finite Element Method. Wiley, Hoboken (2015)
9. Baflon, J.P., Masounave, J.: On the relationship between the parameters of Paris' Law for fatigue crack growth in aluminum alloys. Scr. Metall. **11**, 1102–1106 (1977)